journal

Impedance and AC Conductivity of $GdCr_{1-x}Co_xO_3$ (x = 0, 0.33, 0.5, 0.67 and 1) Perovskites

Margareta Pecovska-Gjorgjevich,[‡,†] Slobotka Aleksovska,[§,¶] Marjan Marinšek,[‖] and
Sandra Dimitrovska-Lazova[§]

[‡]Faculty of Natural Sciences and Mathematics, Department of Physics, "Ss. Cyril and Methodius" University,
Skopje 1000, Macedonia

[§]Faculty of Natural Sciences and Mathematics, Department of Chemistry, "Ss. Cyril and Methodius" University,
Skopje 1000, Macedonia

[¶]Faculty of Medical Sciences, Goce Delcev University, Stip, Macedonia

[‖]Faculty of Chemistry and Chemical Technology, University of Ljubljana, Ljubljana 1000, Slovenia

Perovskite series $GdCr_{1-x}Co_xO_3$ (x = 0, 0.33, 0.5, 0.67 and 1) was obtained using a solution combustion method. The powder XRD was used for identification and structural characterization of the obtained perovskites. All compounds crystallize within the space group *Pnma*. The morphology of samples was studied using SEM. The impedance and AC conductivity of $GdCr_{1-x}Co_xO_3$ were studied using impedance spectroscopy in a frequency range from 10 Hz to 10 MHz and in temperature interval 297–337 K. Changes in electric modulus and DC conductivity, with increasing of the value of x in the structures, were observed. The AC conductivity obeyed the universal power law, $\sigma(\omega) = \sigma(0) + A\omega^n$ and revealed semiconductor behavior. The calculated activation energies of existing processes varied with the cobalt content and applied frequency. The impedance spectra showed non-Debye behavior with a distribution of relaxation times for relaxation and conductive processes. The conduction mechanism for pure orthochromite and orthocobaltite was defined and two types of conduction were observed in the investigated temperature range for the complex perovskites. In order to explain the results, an equivalent circuit with fitted values of circuit components was proposed.

I. Introduction

IN recent decades, perovskite materials have been the subject of growing scientific interest. This is due to the interplay between the variation of perovskite composition and structure, thus tuning the properties that perovskite materials exhibit. Therefore, starting from the general formula of perovskites, ABX_3 (where A, B denote cations, and X is an anion), many different compounds may be derived via combinations of A, B, and X, including the possibility for multiple substitutions in the cationic positions leading to even larger number of compounds.[1] It is well known that perovskites are materials that exhibit a variety of different specific and unique properties (superconductivity, giant magnetic resistance, pyroelectricity, etc.).[2] As to the electrical properties, the literature data indicate that different perovskites show insulating, semiconducting or metal-conducting behaviors depending on the constituent elements, structures, and temperatures.[3,4]

Perovskites containing cobalt or chromium ions in B-position have been subject to many investigations, which have shown that cobalt perovskites ($RCoO_3$) exhibit interesting properties, including high electronic conductivity,[5] metal-to-insulator transition with increasing temperature,[6] significant catalytic activity[7] and specific magnetic properties.[8–10] For $GdCoO_3$, it was found to be a semiconductor at room temperature and that it undergoes semiconductor-to-metal transition at 860 K.[11] The rare earth chromites are also interesting because of their relatively high electrical conductivity, resistance to oxidation, high melting points[12] and multiferroic properties observed in some chromites.[13,14] Moreover, $GdCrO_3$, was reported to behave as a semiconductor in the temperature range of 300–1000 K.[15] However, there are limited data on perovskites containing both Co^{3+} and Cr^{3+} ions in B-position. Recently, we have reported on the electric properties of $YCr_{0.5}Co_{0.5}O_3$.[16] We have also presented the results regarding the synthesis and crystal structures of $RCo_{1-x}Cr_xO_3$ perovskite materials (R = Pr or Gd, x = 0, 0.33, 0.5, 0.67, and 1).[17,18] There are practically no literature data concerning the electric properties of these series of complex Co/Cr perovskites. Therefore, it seemed reasonable to study the dependence of the electrical conductivity on the content of cobalt and chromium in B-site. In this paper, we present the results obtained for the impedance and AC conductivity studies of various $GdCr_{1-x}Co_xO_3$ materials.

II. Experimental Procedure

The investigated series $GdCr_{1-x}Co_xO_3$ was synthesized according to the procedure given in the paper of Dimitrovska-Lazova *et al.*[17] The solution combustion synthesis was performed using water solutions of corresponding metal nitrates and urea as a fuel. The ratio between fuel (urea) and oxidizers (nitrates) was set to one. The self-ignition reaction was performed in muffle furnace preheated to a temperature of ~773 K. The obtained precursors were subsequently calcined at temperature of 1073 K for 4 h.

The purity of obtained perovskites as well as their crystal structures was studied via powder X-ray diffraction. XRD patterns were obtained using a powder diffractometer (Bruker D8 Advance, Tucson, AZ) with CuK_α radiation (Ni-filtered) and detector (SolX) in the range from 10° to 120° 2θ with a step-scanning rate of 0.02°. The microstructures of the obtained compounds were investigated via SEM microscope (Field-Emission FE-SEM Zeiss ULTRA PLUS, Oberkochen,

Germany) using accelerating voltage of 2 kV. The samples were put onto graphite tape and were not gold-sputtered prior to the microscopy. Images were taken using In-lens and/or standard Evernhart–Thornley secondary electron (SE) detectors.

The LCR meter (HP 4192A; Agilent Technologies, Santa Clara, CA) and solid dielectric test fixture (HP 16451B) with four terminal electrodes with 38 mm diameter and a temperature chamber, were used for the dielectric measurements at parallel mode and impedance measurements at serial mode. The AC voltage was 1 V. The flat surfaces of the pellets were electroded using high purity silver paste. The dielectric parameters capacitance (C_p) and dielectric losses (tanδ), were measured as a function of frequency (10 Hz–10 MHz) and of temperature (297–337 K). The obtained data were further used for estimation of complex electric modulus, real, and AC conductivity. The experimental data of the real and imaginary part of complex impedance were used to deduce the electrical characterization of the materials and to propose an equivalent circuit for possible conduction mechanisms.

III. Results and Discussion

(1) Structural and Morphological Analysis

The crystal structures of the end members of the series (GdCoO$_3$ and GdCrO$_3$) have been reported previously.[12,19–24] Additionally, the thorough investigation of the crystal structure of the whole GdCr$_{1-x}$Co$_x$O$_3$ (x = 0, 0.33, 0.5, 0.67, and
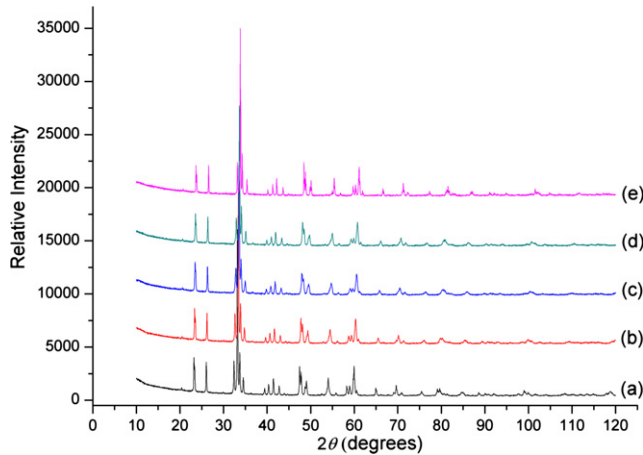

Fig. 1. XRD patterns of (a) GdCrO$_3$; (b) GdCr$_{0.67}$Co$_{0.33}$O$_3$; (c) GdCr$_{0.5}$Co$_{0.5}$O$_3$; (d) GdCr$_{0.33}$Co$_{0.67}$O$_3$; (e) GdCoO$_3$.

1) series, obtained via a solution combustion method, was the subject of our work.[17] Here, only the most important structural characteristics related and relevant to this work will be presented.

The XRD patterns of the GdCr$_{1-x}$Co$_x$O$_3$ series are represented in Fig 1, showing a continuous shift of the positions of the diffraction peaks toward higher values with increasing x value, as the larger Cr^{3+} is substituted with the smaller Co^{3+} ion. Thus, an isomorphous series of pure perovskite phases was obtained with negligible amounts of Co$_3$O$_4$ in GdCr$_{0.5}$Co$_{0.5}$O$_3$ and GdCr$_{0.33}$Co$_{0.67}$O$_3$. The Rietveld refinements of the crystal structures showed that the members of GdCr$_{1-x}$Co$_x$O$_3$ series crystallize in the orthorhombic *Pnma* space group with Z = 4. The lattice parameters and selected distances and angles are given in Table I. The relationship between the unit cell parameters in these compounds ($b > c/\sqrt{2} > a$) is the same as in O-type perovskites in which the tilting of the octahedra is the primary source of distortion from the ideal cubic structure. The calculated cell distortion and orthorhombic distortion[17] indicate that the unit cell distortion decreases with increasing Co content.

According to the average values of the Gd–O distances (Table I), which are decreasing with the subsequent substitution of Cr^{3+} with Co^{3+}, it could be concluded that the coordination number of Gd^{3+} cation is 10 in GdCoO$_3$, but nine in all other members of the series. It must be also emphasized that the octahedrons become increasingly distorted as the content of Co^{3+} increases, but they are simultaneously less tilted. An important physical characteristic for perovskites is the so-called global instability index,[25] calculated on the bases of bond valences.[26–28] The calculated global instability indices[17] indicated the existence of lattice-induced strains in the structure of the cobalt containing compounds, while GdCrO$_3$ is a structure almost without any internal stress.

The SEM images of the surfaces for GdCr$_{1-x}$Co$_x$O$_3$ are shown in Fig. 2. Shapes are clearly visible, indicating the existence of polycrystalline porous microstructure, typical for perovskites obtained by solution combustion method. The pure orthochromite sample (a) is characterized by slightly elongated spherical grain morphology. Individual grains are of relatively narrow size distribution with an average size of ~150 nm. The addition of cobalt results in grain growth, so the crystals appear to be less uniform in both size and shape. The average grain size changes from the initial ~150 nm for GdCrO$_3$ to ~300, ~400, and ~450 nm for GdCr$_{0.67}$Co$_{0.33}$O$_3$, GdCr$_{0.5}$Co$_{0.5}$O$_3$ and GdCr$_{0.33}$Co$_{0.67}$O$_3$, respectively, and reaches the final value of approximately 550 nm for GdCoO$_3$. Grains retain slightly elongated spherical shapes up to

Table I. Unit Cell Parameters, Average A, B–O Distances, Deformation of Unit Cell (*d*), Orthorhombic Distortion (*dist*$_{orth}$), Tilt Angles, Global Instability Index, Crystallographic Density and Porosity of GdCr$_{1-x}$Co$_x$O$_3$ Perovskites

| Parameters	GdCrO$_3$	GdCr$_{0.67}$Co$_{0.33}$O$_3$	GdCr$_{0.5}$Co$_{0.5}$O$_3$	GdCr$_{0.33}$Co$_{0.67}$O$_3$	GdCoO$_3$
a (Å)	5.52447 (12)	5.4832 (2)	5.4573 (3)	5.4357 (3)	5.39074 (12)
b (Å)	7.60552 (16)	7.5572 (3)	7.5280 (4)	7.5046 (4)	7.45514 (17)
c (Å)	5.31310 (11)	5.2850 (2)	5.2685 (3)	5.2541 (3)	5.22527 (12)
$<$Gd–O$>_9$ (Å)	2.530 (2)	2.517 (2)	2.507 (2)	2.500 (3)	2.490 (3)
$<$B–O$>_6$ (Å)	1.983 (2)	1.969 (2)	1.957 (2)	1.953 (3)	1.930 (3)
B-O1-B (°)	148.85 (8)	149.30 (9)	151.76 (9)	150.84 (11)	153.60 (10)
B-O2-B (°)	149.2 (2)	149.5 (3)	149.6 (3)	149.2 (4)	151.2 (4)
d	2.677	2.395	2.199	2.048	1.731
$dist_{orth}$	0.2914	0.2905	0.2901	0.2900	0.2892
Δ_6	0.044	0.014	0.103	0.134	0.138
θ (°)	15.493	15.283	14.116	14.131	13.722
ϕ (°)	10.571	10.62	10.362	9.763	9.931
Φ (°)	18.683	18.538	17.448	17.119	16.882
GII	0.054	0.161	0.183	0.189	0.199
Crystallographic density (g/cm^3)	7.654	7.873	8.001	8.117	8.356
Porosity (%)	38.0	40.4	40.9	41.6	42.0
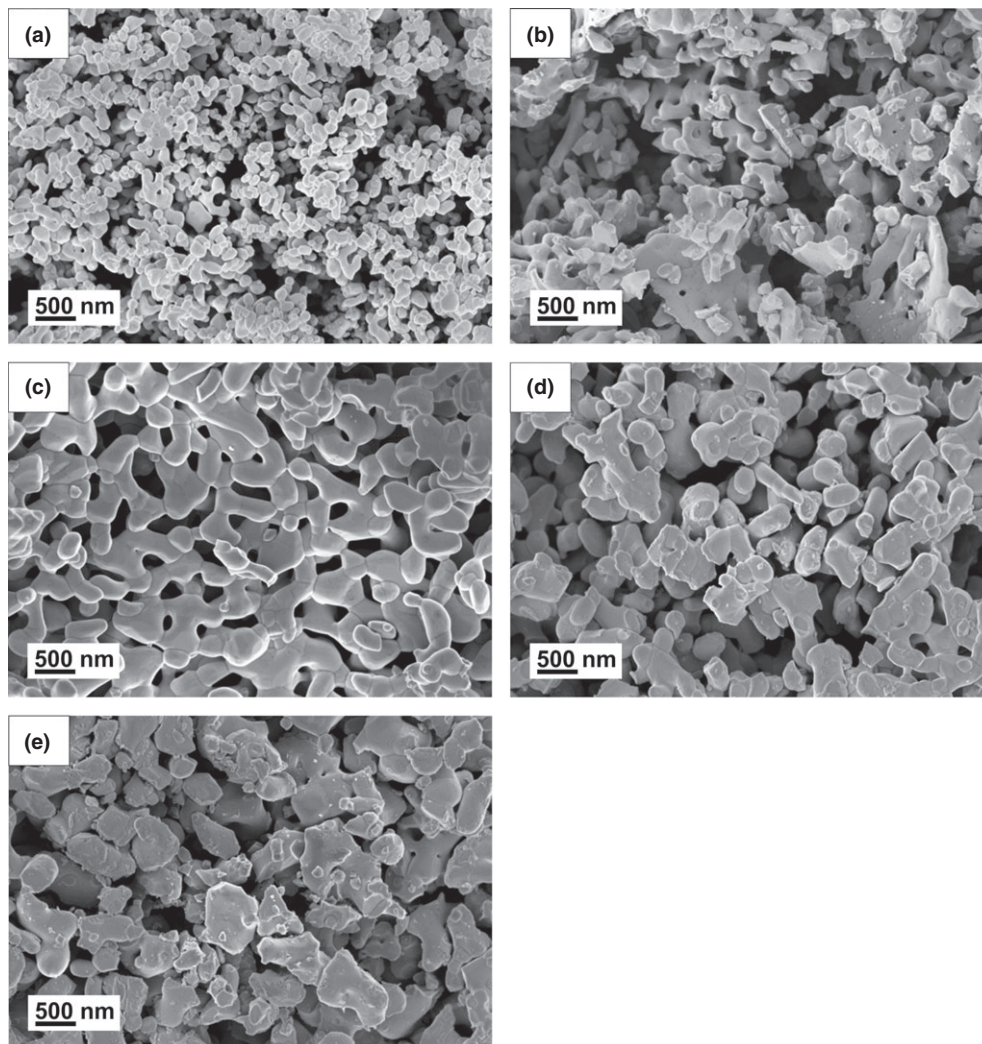
Fig. 2. Microstructure of $GdCr_{1-x}Co_xO_3$, $x = 0$, 0.33, 0.5, 0.67 and 1 for (a), (b), (c), (d) and (e), respectively.

$x = 0.5$. At higher x values, individual grains exhibit sharp edges and thus become less regular. Grains with sharp edges are normally an indication of lower combustion temperature during the $GdCr_{1-x}Co_xO_3$ synthesis. An interesting result was obtained for $GdCr_{0.5}Co_{0.5}O_3$ where grains and grain boundaries are almost equally represented with almost uniform size.

(2) Electric Modulus Analysis

In order to review what is happening in the bulk material and to separate the conduction processes in the low frequency region, the electric modulus formalism was applied, which is a highly appropriate method introduced by Macedo,[29] and is used whenever one cannot extract any information from the dielectric constant and loss measurements about the polarization processes involved in the structures. With this method, the electrode polarization effect or mobile ion polarization are suppressed and the conductivity coming from the material is the only process observed. The electric modulus corresponds to the relaxation of the electric field in the material when the electric displacement remains constant.[30]

Complex electric modulus is defined as reciprocal of the complex permittivity:[31]

$$M^* = 1/\varepsilon^* = M' + iM'' \tag{1}$$

where M^* is the complex modulus, ε^* is the complex permittivity, M' and M'' are real and imaginary parts of the

modulus, respectively. For pure conduction process, the relaxation peak in the modulus plot would be observed, while no peak would appear in corresponding ε'' plot. If the dielectric relaxation process is present, a relaxation peak would appear in both M^* and ε^* representation.[32,33]

The frequency dependence of the imaginary part M'' of complex modulus for all five investigated structures is shown in Fig. 3. The spectra showed a broad and asymmetric non-Debye behavior peaks with distribution of relaxation times around the M'' peak position frequency and incoming another peak at higher frequencies. These peaks define the transition from ion hopping from one site to the neighboring
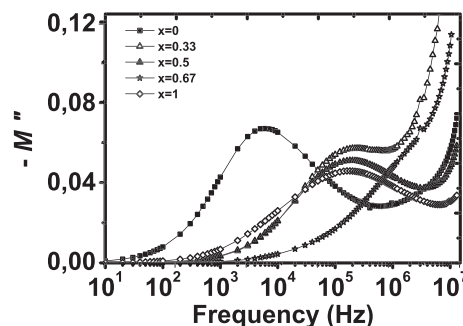

Fig. 3. Frequency dependence of imaginary part of complex electric modulus at 297 K.

site in low frequency range and long-range mobility to high frequency short mobility range connected with localized motion of the ions.

The mean relaxation times of the relaxation processes for all five investigated structures were calculated from the frequencies of the maximum points of the curves, $(\tau \sim \omega_m^{-1})$. The highest value of τ (26.54 µs) was observed for GrCrO$_3$. For other samples, the calculated τ values were similar and ranged in the interval 0.7238 − 0.8846 µs. The relatively high τ value for GrCrO$_3$ in comparison to the other members of the series might be due to the highest deviation of B–O1/O2–B angles from 180° in its structure (Table I). It is expected that the magnitude of the orbital overlaps is determined by the deviation angle as well as the nature of ions.[34] Thus, with decreasing orbital overlap (which means higher deviation from 180°), there is an expected increase in resistivity, since the band gap between the conduction and the valence bands becomes greater.

Figure 4 shows the frequency dependence of M' (a) and M'' (b) for GdCrO$_3$ at various temperatures. The relaxation peak observed for M'' is shifted toward higher frequencies with increasing temperature, and its magnitude is increased, i.e., the relaxation rate for this process increased with heating. The characteristic relaxation times calculated from the frequency of the peak position were also fitted to the Arrhenius law, $\tau = \tau_0 \exp(E_a/k_B T)$, where τ is relaxation time, k_B is Boltzman constant, E_a is activation energy of the thermal process, and T is absolute temperature. The obtained values of activation energies for the series are in interval 1.1 eV for $x = 1$ to 0.8 eV for $x = 0$. The decrease of activation energy with increasing cobalt content was established. The observed activation energies of conduction processes could be connected to the space charge model, which gives activation energies in interval 1.07−1.48 eV. This model was used in explanation of the dielectric relaxation phenomena in several perovskite materials.[34,35]

(3)   Conductivity Study
Properties, such as real and imaginary part of the complex permittivity, dielectric losses and electrical conductivity, are closely related to the microstructure of the material and its composition. Conductivity behavior of the prepared series depending on frequency and temperature was also investigated. The observed total conductivity was a sum of AC conductivity, which came from a reversible hopping between two states, and DC conductivity, which emerged from a percolation path through the sample.

The porosity in the structures is evident from the SEM photographs (Fig. 2), and has to be considered in further analysis of the electric conductivity. It shows the presence of the grain boundaries which affect the electrical behavior of the structures.[15] The porosity of the pellets was calculated from the theoretical crystallographic[36] and the experimental density of the pellets and is in interval between 38% and 42%. The porosity slightly increases with increasing cobalt amount in perovskite structures (Table I). For two-phase systems consisting of an electrically conductive (perovskite) and nonconductive (porosity) phase, the corrected electrical conductivity of the bulk, σ_p, was calculated from the formula:[37]

$$\sigma_{eff} = \frac{3}{2}\sigma_p\left(1 - por - \frac{1}{dim}\right) \quad (2)$$

where σ_{eff} is the experimental value of the pellet conductivity, por is the fraction of porosity $(1 - d_{exp}/d_T)$ and dim is three for the three-dimensional system. The corrected value of electrical conductivity is of the same order of magnitude as the measured one, so it could be concluded that in the investigated temperature range, the presence of grain boundaries has no significant influence on the conductivity. This conclusion is in agreement with the literature data,[15] where the changes in the bulk conductivity coming from the grain boundaries are significant over 500 K.

The frequency-dependent conductivity spectra of all structures measured at room temperature are shown in Fig. 5(a). The experimental data are shown as a plateau in the low frequency region defined as σ_{dc} and the exhibited dispersion is directly dependent on the frequency changes at high frequencies. The width of the plateau region varied with cobalt content. Mixed structures, GdCr$_{1-x}$Co$_x$O$_3$, exhibited higher σ_{dc}
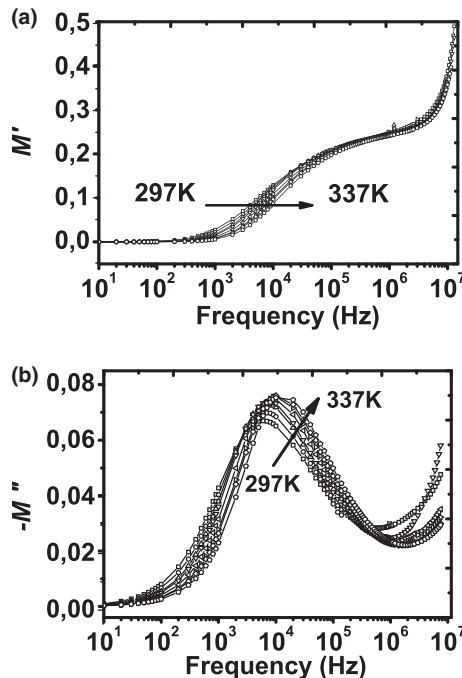

Fig. 4.   Frequency dependence of (a) real and (b) imaginary parts of complex electric modulus for GdCrO$_3$ at temperature interval 297–337 K.
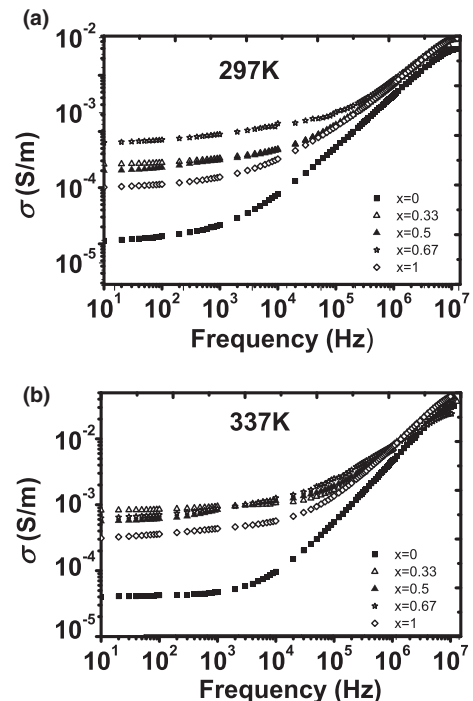

Fig. 5.   Frequency-dependent conductivity of GdCr$_{1-x}$Co$_x$O$_3$ series for (a) 297 K; (b) 337 K.

values than $GdCrO_3$ and $GdCoO_3$. The σ_{dc} of $GdCoO_3$ was higher than the σ_{dc} of $GdCrO_3$.

The DC conductivity was dominant in the low frequency region until the hopping frequency ω_h (the frequency when conductivity doubles σ_{dc}) was reached. At frequencies higher than the hopping frequency ω_h, AC conductivity became dominant. The AC conductivity increased with increasing frequency and the curves were merged at high frequencies. The data were fitted to Jonscher's power law:[38] $\sigma(\omega) = \sigma(0) + A\omega^n$, where $\sigma(0)$ is the DC conductivity σ_{dc} which is frequency independent, A is the preexponential factor and n is the power law exponent with values $0 < n < 1$. The parameter n characterizes the interaction between the charge carriers participating in the polarization process and the value $n = 1$ indicates an ideal case of Debye behavior when no interaction happens. The lower value of n defines stronger ion–ion coupling.[39] The obtained n values were in the 0.65–0.87 range and were dependent on cobalt content. The highest value (0.84–0.87) was obtained for $GdCrO_3$. For the complex perovskites (Co/Cr), the values of n were decreased with increasing content of cobalt (0.71–0.76 for $x = 0.33$; 0.66–0.73 for $x = 0.5$ and 0.39; 0.52 for $x = 0.67$), but for the pure orthocobaltite n value was again increased (0.75–0.78). The data for pure orthochromite and orthocobaltite were close to the predicted value for temperature independent n (around 0.8).[40,41]

Figure 5(b) shows the frequency-dependent conductivity behavior of all structures at 337 K. The most noticeable increase of total conductivity was observed for $GdCrO_3$ and the lowest changes of σ were for $GdCr_{0.33}Co_{0.67}O_3$, i.e. the structure that already showed high conductivity (grain boundary conduction mechanism was dominant in all temperature range). The difference between $GdCrO_3$ and $GdCoO_3$ remained one order of magnitude. This behavior is expected because grain boundaries for pure structures ($x = 0$, 1) appear at higher temperatures, while for the mixed structures they participate to the conductivity at lower temperatures.

The DC conductivity is increasing with temperature, which confirmed the semiconducting behavior of the materials. The activation energies estimated from the Arrhenius plots in accordance to the relation $\sigma_{dc}(T) = A\exp(-E_a/k_{BT})$ were 0.278, 0.258, 0.202, 0.220, and 0.223 eV for $x(Co) = 0$, 0.33, 0.5, 0.67 and 1, respectively and are in good agreement with the literature.[15,42] Activation energy also showed decreasing dependence with the increasing amount of cobalt in the structures, showing the lowest value for $x = 0.5$. According to the study of Subba Rao,[42] the energy bands associated with rare earth ions are not relevant to the electrical conduction in $RCrO_3$. He suggested the existence of a large number of Cr^{4+} centers due to native defects in $RCrO_3$ and the conduction of holes from these centers to neighboring Cr^{3+} sites. However, the literature data point out that for $RCoO_3$, the spin state of Co^{3+} and the temperature of LS-IS-HS transitions depend on the rare earth cation.[8] Thus, as the rare earth becomes smaller the progressive stabilization of $\pi^*(Co-O)$ levels and large splitting between t_{2g} and e_g orbitals is obeserved.[43] Therefore, the transitions to higher spin configurations take place at higher temperatures. Taking into consideration that $GdCoO_3$ undergoes spin transition at 717 K[9] and that the temperature range in our investigation is rather narrow and the maximum temperature is 337 K, it could be concluded that Co^{3+} must be in its low spin state.

The values of activation energies lead to the conclusion that conduction is extrinsic and is of the hole-hopping type.[15] Since the electrical conduction is directly connected to the energy bands of the B-cation in the structure, the changes in the conductivity are directly connected to the cobalt content. The explanation could be found in the electronic configuration of the two cations in the B-site, i.e., replacing of Cr^{3+} $(t_{2g}^3 e_g^0)$ with Co^{3+} $(t_{2g}^6 e_g^0$ in low-spin state, $S = 0)$.[43]
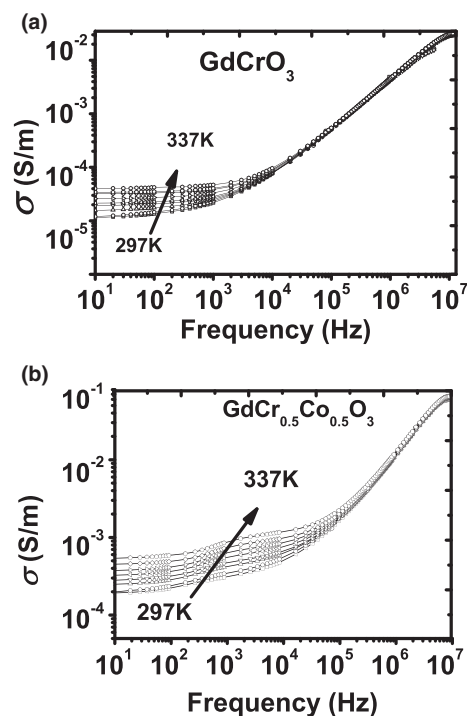
(a)

(b)

Fig. 6. Frequency-dependent conductivity at various temperatures for (a) $GdCrO_3$; (b) $GdCr_{0.5}Co_{0.5}O_3$.

Taguchi established the importance of the cation–anion–cation overlap in the electrical properties of perovskites of this type.[44] The ionic radius of Co^{3+} ion in the high-spin state is nearly equal to the ionic radius of the Cr^{3+} ion and this would not change the conductivity with increasing x.[45] The decrease of (Cr,Co)-O distance and increasing conductivity in $GdCr_{1-x}Co_xO_3$ with increasing x suggests that Co^{3+} ion must have been in the low-spin state (t_{2g}^6). So the increasing amount of smaller Co^{3+} led to stronger π bonding (overlap between the cation d and oxygen p_π orbitals), which resulted in higher conductivity.

The frequency dependences of total conductivity at various temperatures for $GdCrO_3$ (a) and $GdCr_{0.5}Co_{0.5}O_3$ (b) are shown in Fig. 6. In the low frequency region, the results are dictated by the behavior of DC conductivity, whereas at higher frequencies, the power law is preserved. Conductivity increased with increasing temperature showing that the semiconductor behavior and the hopping frequency ω_h (the point of changing the conductivity from DC to AC) are shifted to higher frequencies. The lowest value of conductivity was observed for $GdCrO_3$ (the structure of lowest global instability index), and the highest for $GdCr_{0.33}Co_{0.67}O_3$, presumably the structure with the highest amount of conductive defects. The changes of the conductivity behavior for complex perovskites in this temperature interval are connected to the grain boundaries contribution, whereas dominant conductive mechanism for $GdCrO_3$ and $GdCoO_3$ is through the grains.

The above statements are consistent with the data from SEM (Fig. 2). For $GdCrO_3$ and $GdCoO_3$ morphologies with dominant grains over grain boundaries are observed, allowing easy passage of the charge carriers from grain to grain and confirming highly conductive nature of $GdCrO_3$ and $GdCoO_3$. The structure of $GdCrO_3$ was more compact, with smaller grains, and it gave a lower value for conductivity than the structure of $GdCoO_3$. The free space between the grains increased with higher content of Co, thus also increasing the contribution of the grain boundaries to the overall conductivity. This is observed for $GdCr_{0.5}Co_{0.5}O_3$ [Fig. 6(b)], with two plateaus at low frequencies, one for the grain and one for the grain-boundary contribution to the conductivity.

(4) Impedance Spectra

Using an AC impedance analysis, it is possible to distinguish between the grain boundary, bulk and grain-electrode effects, which usually define the sites of traps for oxygen vacancies and other defects. Moreover, from the relaxation processes that take place in the material, the contributions to the total conductivity coming from the bulk, the grain-boundary, and the space charge polarization could be defined.

Figure 7 shows the frequency dependence of Z' and $-Z''$ for GdCrO$_3$ (a) and GdCr$_{0.5}$Co$_{0.5}$O$_3$ (b) as a function of temperature. The decrease of Z' with increasing frequency for temperatures implies that the relaxation process in the structures was observed. The magnitude of Z' in the low frequency range decreased with increasing temperature, which is attributed to the reduction of grains, grain boundaries, and the electrode interface resistance. This is clearly shown in the graph of GdCr$_{0.5}$Co$_{0.5}$O$_3$ where different slopes with knees connected to grain and grain boundaries are observed. All curves merged at frequencies higher than 10 kHz, indicating space charge releasing and increasing the conductivity in the structures.

From the frequency dependence of $-Z''$, given on the same figure, only one peak for GdCrO$_3$ could be noticed. Such behavior is similar for all samples except for $x = 0.5$, where another peak appears. The first peak at lower frequencies for GdCr$_{0.5}$Co$_{0.5}$O$_3$ corresponds to grain boundary resistance and the second peak at higher frequencies to bulk resistance.

The positions of the peaks were set to the center of the dispersion region of Z'. The values for GdCrO$_3$ and GdCoO$_3$ showed higher impedance in comparison to the other samples, thus revealing a more stable structure of pure perovskites. A relatively low value of resistance was observed for $x = 0.67$, which confirmed the high conductivity recorded for this sample. The reason for higher conductivity of this sample may be in the high content of grain boundaries. The frequencies for the peak positions were defined as the frequencies for grain and grain boundary relaxation processes (see the analysis from the conductivity and electric modulus).

The degreasing of $-Z''$ peak with increasing temperature is also observed. It was noticed that the influence of grain boundary to the resistance increased and became dominant with increasing temperature. However, the relative increase of grain boundary resistance was less than the relative decrease of grain bulk resistance, which led to the overall increasing of conductivity with increasing temperature.

A shift of the peak positions to the higher frequency side defines a thermally activated relaxation time, which obeyed Arrhenius' law, $\tau = \tau_0 \exp(E_a/k_{BT})$. The activation energy (E_a) obtained from the Arrhenius plot was estimated to 0.36 eV for GdCrO$_3$; 0.33 eV for GdCr$_{0.67}$Co$_{0.33}$O$_3$; 0.44 eV for GdCr$_{0.33}$Co$_{0.67}$O$_3$ and 0.50 eV for GdCoO$_3$. For GdCr$_{0.5}$Co$_{0.5}$O$_3$, two activation energies are estimated: 0.43 eV for conductivity through grains and 0.25 eV for conductivity through grain boundaries.

The peak frequencies $\omega_{M''}$ in M'' curves, Fig. 3, were higher than $\omega_{Z''}$ in Z'' curves, Fig. 7. This corresponds to lower relaxation times for dielectric process related to the relaxation times for the conduction process estimated from impedance measurements. Different results for activation energies obtained from M'' and Z'' defined different processes in the bulk, conductive and dielectric relaxation.

(5) Impedance Spectra Fitting

Figure 8 shows the dependence of the imaginary versus real part of the complex impedance, also called the Nyquist plot, for all five structures at 297 K (a) and 337 K (b). The results showed deformed semicircles revealing the Debye behavior at high frequencies, where the angle of the intersect of arcs with the real axis is 90°, whereas the angle of the intersect at low frequencies is less than 90° and is temperature dependent. Only GdCr$_{0.5}$Co$_{0.5}$O$_3$ showed two clear separate semicircles, confirming the presence of two different dispersion mechanisms in the structure, which is not clear in other structures.

The experimental data corresponded to the equivalent circuit proposed by B. A. Boukamp,[46] which comprised three elements connected in series assigned to bulk, grain boundary, and electrode contributions [Inset of Fig. 8(a)]. Each of the elements is composed of parallel connected resistors and a constant phase element (CPE) for grain or grain boundary (first two elements); or resistance and capacitor for electrode
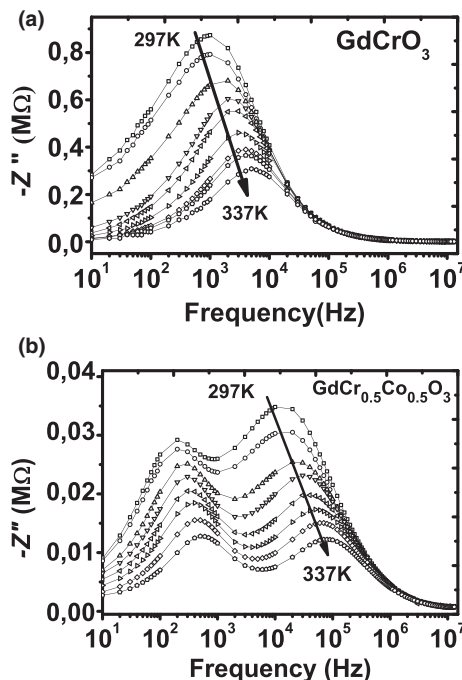

Fig. 7. Frequency dependence of Z' and $-Z''$ of (a) GdCrO$_3$; (b) GdCr$_{0.5}$Co$_{0.5}$O$_3$ at various temperatures.
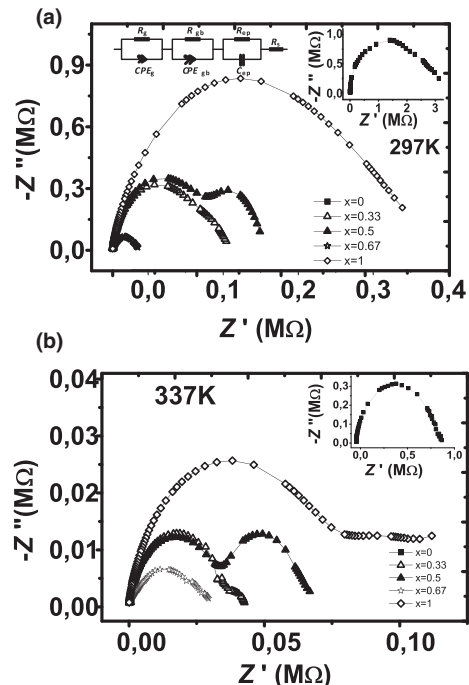

Fig. 8. Nyquist diagrams for all samples at (a) 297 K; (b) 337 K. The inset graph is for GdCrO$_3$. Equivalent circuit for GdCr$_{1-x}$Co$_x$O$_3$ is embedded in (a).

contributions (third element). The presence of CPE is due to the observed wide peak of $-Z''$ that defines the distribution around the mean relaxation time. In this proposed model, the complex impedance is expressed by the equation:

$$Z^*(\omega) = Z^*_{bulk} + Z^*_{gb} + Z^*_{ep}$$

$$Z^*_{bulk} = \frac{R_g}{1 + A_0 R_g (i\omega)^n} \qquad Z^*_{gb} = \frac{R_{gb}}{1 + B_0 R_{gb}(i\omega)^m}$$

$$Z^*_{ep} = \frac{R_{ep}}{1 + i\omega R_{ep}}, \tag{3}$$

where A_0, B_0, n and m are temperature-dependent parameters.

The point of intersection of the high frequency arc with the real impedance axis at high frequency side, defined the serial resistance of the circuit R_s, which was small and negligible to the overall resistance. The difference between two intersect points of the semicircles gave the bulk (grain) resistance of the material R_g and the corresponding CPE_b was calculated from the frequency of the highest point in the arc. The similar calculation of grain boundary resistances R_{gb} and CPE_{gb} was performed on second semicircles which appeared with increasing temperature. The resulted semicircles were not ideal, but depressed and their centers were below the real axis. Mixed structures revealed grain boundary effect, second arc in the Figs. 8(a) and (b), at lower temperatures than GdCrO$_3$ and GdCoO$_3$ (most noticeable for $x = 0.5$). The difference from ideal arc in the low frequency region was ascribed to the presence of the electrode polarization process, which was not well defined because of measuring limitations. The value of the bulk resistance calculated from the impedance plot for GdCrO$_3$ is found to be higher by one order of magnitude than that of GdCoO$_3$ and it decreased with mixing Cr and Co, while grain boundary resistance increased.

The fitting results revealed the presence of the $R_g CPE_g$ parallel circuit and also the secondary grain boundary $R_{gb}CPE_{gb}$ parallel circuit masked in the large semicircle of bulk resistance. The estimated values of CPE_b and CPE_{gb} are in the order of 0.02 nF for grains and 0.2 nF for grain boundaries, respectively, and were decreasing with increasing temperature. The fitted values of capacitance C_{ep} were in the order of 10 nF. The grain boundaries contributed to the ionic transport and increased the conductivity due to the presence of a large density of defects in the interfacial region or the imperfect lattices of investigated structures.[47–49]

The influence of the temperature on separation of the two circles is evident. The grain boundary resistance increased, respectively, to grain resistance with the increasing temperature, revealing the increasing influence of grain boundaries on total conductivity in all samples. The values of R_{ep} were not defined since the arcs at the low frequency region were not sufficiently clear for accurate estimations.

The results of the temperature-dependent complex impedance spectra for GdCrO$_3$ and GdCr$_{0.5}$Co$_{0.5}$O$_3$ are presented in Figs. 9(a) and (b). The arcs were broad, depressed and extended to the coordinate origin at all investigated temperatures confirming the non-Debye behavior from before. Only one arc for GdCrO$_3$ [Fig. 9(a)], due to a bulk transport mechanism was present but another relaxation process with mean time constant close to the main one appeared to be masked. This relaxation process influenced the distortion of the experimental arc. The second arc appeared at higher temperatures and connected to the transport mechanism through grain boundaries. The reducing of the resistance value with increasing temperature revealed the negative resistance coefficient, similar to the results from the conductivity study. The presence of two arcs in the whole temperature range (higher impact of grains over grain boundaries at lower temperatures) was observed for GdCr$_{0.5}$Co$_{0.5}$O$_3$ with increasing influence of grain boundaries at higher temperatures.
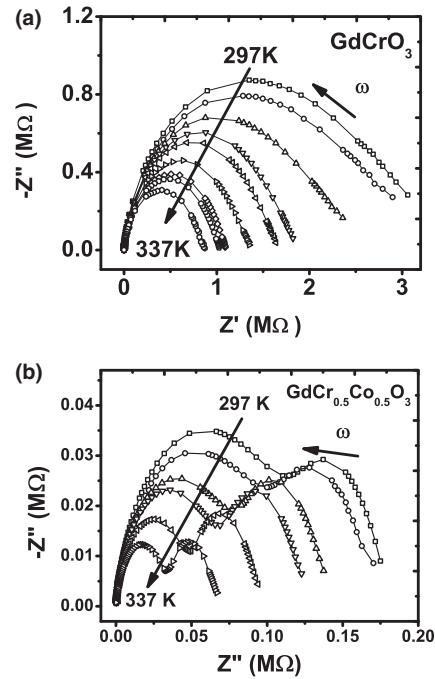

Fig. 9. Nyquist plot of complex impedance at various temperatures for (a) GdCrO$_3$ and (b) GdCr$_{0.5}$Co$_{0.5}$O$_3$.

IV. Conclusion

The dielectric response of the prepared perovskite series GdCr$_{1-x}$Co$_x$O$_3$ ($x = 0$, 0.33, 0.5, 0.67, and 1) was studied with dielectric spectroscopy, and the experimental data were analyzed by means of electric modulus formalism, conductivity studies, and impedance spectroscopy analysis.

The relaxation processes in GdCrO$_3$ observed in complex modulus dependences, connected to broad and asymmetric non-Debye behavior peaks of relaxation processes, had a higher value of mean relaxation time than in other structures. The smaller values of τ were connected with the presence of cobalt in the structures. Decreasing of activation energies for relaxation processes also showed the influence of cobalt increasing in the structures.

AC and DC conductivity also increased with increasing x. The structures were defined as electronic conductors, with p-type extrinsic semiconducting behavior in the studied temperature range. The spin state of Co^{3+} ions was assumed as low (t_{2g}^6), which influenced the conductivity of the structures with increasing x. The increasing amount of Co^{3+} led to increasing number of $3d$ electrons of the B-site cation and stronger π bonding, which resulted in higher conductivity, mostly observed for mixed structures ($x = 0.5$ and 0.67). The higher conductivity is also connected to the increasing of internal stress, i.e., global instability indices. All structures' conductivities obeyed the universal power law.

Impedance spectra showed similar behavior as complex electric modulus, non-Debye behavior with distribution of relaxation times. The grain boundaries contribution to overall impedance, beside grain resistance was more pronounced for mixed structures at lower temperatures and for GdCr$_3$ and GdCoO$_3$ at higher temperatures.

The equivalent circuit was proposed in order to define grain and grain boundary resistances, and the corresponding capacitances.

References

[1]R. H. Mitchell, *Perovskites: Modern and Ancient*. Almaz press, Thunder Bay, 2002.
[2]F. S. Galasso, *Perovskites and High T$_c$ Superconductors*. Gordon and Breach Science Publishers, New York, 1990.

[3]C. N. R. Rao, "Transition Metal Oxides," *Annu. Rev. Phys. Chem.*, **40**, 291–326 (1989).

[4]A. S. Bhalla, R. Guo, and R. Roy, "The Perovskite Structure – A Review of Its Role in Ceramic Science and Technology," *Mat. Res. Innov.*, **4**, 3–26 (2000).

[5]T. Ishihara, "Structure and Properties of Perovskite Oxides"; Chapter 1, pp. 1–16 in *Perovskite Oxide for Solid Oxide Fuel Cells*, Edited by T. Ishihara. Springer, Dordrecht, 2009

[6]S. Yamaguchi, Y. Okimoto, and Y. Tokura, "Bandwidth Dependence of Insulator-Metal Transitions in Perovskite Cobalt Oxides," *Phys. Rev. B*, **54** [16] 11022,4 pp (1996).

[7]M. A. Peña and J. L. G. Fierro, "Chemical Structures and Performance of Perovskite Oxides," *Chem. Rev.*, **101**, 1981–2017 (2001).

[8]A. Fondado, J. Mira, J. Rivas, C. Rey, M. P. Breijo, and M. A. Señarís-Rodríguez, "Role of the Rare-Earth on the Electrical and Magnetic Properties of Cobalt Perovskites," *J. App. Phys.*, **87** [9] 5612–4 (2000).

[9]K. Knížek, Z. Jirák, J. Hejtmánek, M. Veverka, M. Maryško, G. Maris, and T. T. M. Palstra, "Structural Anomalies Associated with the Electronic and Spin Transitions in LnCoO₃," *Eur. Phys. J. B*, **47**, 213–20 (2005).

[10]H. W. Brinks, H. Fjellvåg, A. Kjekshus, and B. C. Hauback, "Structure and Magnetism of $Pr_{1-x}Sr_xCoO_{3-d}$," *J. Solid State Chem.*, **147**, 464–77 (1999).

[11]S. V. Kurgan, G. S. Petrov, L. A. Bashkirov, and A. I. Klyndyuk, "Properties of $Nd_{1-x}Gd_xCoO_3$ Solid Solutions," *Inorg. Mater.*, **40** [11] 1224–8 (2004).

[12]M. V. Kuznetsov and I. P. Parkin, "Convenient, Rapid Synthesis of Rare Earth Orthochromites LnCrO₃ by Self-Propagating High-Temperature Synthesis," *Polyhedron*, **17** [25–26] 4443–50 (1998).

[13]J. R. Sahu, C. R. Serrao, N. Ray, U. V. Waghmare, and C. N. R. Rao, "Rare Earth Chromites: A New Family of Multiferroics," *J. Mater. Chem.*, **17**, 42–4 (2007).

[14]A. K. Zvezdin and A. A. Mukhin, "Magnetoelectric Interactions and Phase Transitions in a New Class of Multiferroics with Improper Electric Polarization," *JETP Lett.*, **88** [8] 505–10 (2008).

[15]A. K. Tripathi and H. B. Lal, "Electrical Transport in Light Rare-Earth Orthochromites," *J. Mater. Sci.*, **17**, 1595–609 (1982).

[16]M. Pecovska-Gjorgjevich, S. Aleksovska, and S. Dimitrovska-Lazova, "Impedance Spectroscopy Analysis of YCrO₃ and YCo₀.₅Cr₀.₅O₃," *Phys. Macedonica*, **61**, 27–38 (2012).

[17]S. Dimitrovska-Lazova, D. Kovacheva, and P. Tzvetkov, "Structural Characteristics of $GdCo_{1-x}Cr_xO_3$ (x = 0, 0.33, 0.5, 0.67, 1) Perovskites," *Bulg. Chem. Commun.*, **44**, 47–54 (2012).

[18]S. Dimitrovska-Lazova, D. Kovacheva, S. Aleksovska, M. Marinšek, and P. Tzvetkov, "Synthesis and Structural Details of Perovskites Within the Series $PrCo_{1-x}Cr_xO_3$ (x = 0, 0.33, 0.5, 0.67 and 1)," *Bulg. Chem. Commun.*, **44**, 37–46 (2012).

[19]P. S. Devi, "Citrate Gel Processing of the Perovskite Lanthanide Chromites," *J. Mater. Chem.*, **3**, 373–9 (1993).

[20]K. Sardar, M. R. Lees, R. J. Kashtiban, J. Sloan, and R. I. Walton, "Direct Hydrothermal Synthesis and Physical Properties of Rare-Earth and Yttrium Orthochromite Perovskites," *Chem. Mater.*, **23**, 48–56 (2011).

[21]K. Yoshii, "Magnetic Properties of Perovskite GdCrO₃," *J. Solid State Chem.*, **159**, 204–8 (2001).

[22]S. V. Kurgan, G. S. Petrov, L. A. Bashkirov, and A. I. Klyndyuk, "Properties of $Nd_{1-x}Gd_xCoO_3$ Solid Solutions," *Inorg. Mater.*, **40**, 1224–8 (2004).

[23]W. Wei-Ran, X. Da-Peng, S. Wen-Hui, D. Zhan-Hui, X. Yan-Feng, and S. Geng-Xin, "Raman Active Phonons in RCoO3 (R = La, Ce, Pr, Nd, Sm, Eu, Gd, and Dy) Perovskites," *Chin. Phys. Lett.*, **22**, 2400–2 (2005).

[24]A. Jaiswal, R. Das, S. Adyanthaya, and P. Poddar, "Synthesis and Optical Studies of GdCrO₃ Nanoparticles," *J. Nanopart. Res.*, **13**, 1019–27 (2011).

[25]M. W. Lufaso and P. M. Woodward, "Prediction of the Crystal Structures of Perovskites Using the Software Program SpuDS," *Acta Crystallogr.*, **57**, 725–38 (2001).

[26]I. D. Brown and D. Altermatt, "Bond-Valence Parameters Obtained from a Systematic Analysis of the Inorganic Crystal Structure Database," *Acta Crystallogr.*, **41**, 244–7 (1985).

[27]I. D. Brown, "Recent Developments in the Methods and Applications of the Bond Valence Model," *Chem. Rev.*, **109**, 6858–919 (2009).

[28]N. E. Brese and M. O'Keeffe, "Bond-Valence Parameters for Solids," *Acta Crystallogr.*, **47**, 192–7 (1991).

[29]P. B. Macedo, C. T. Moynihan, and R. Bose, "The Role of Ionic Diffusion in Polarization in Vitreous Ionic Conductors," *Phys. Chem. Glasses*, **13**, 171–9 (1972).

[30]A. Dutta, C. Bharti, and T. P. Sinha, "Dielectric Relaxation and AC Conductivity Study in $SrMg_{1/3}Nb_{2/3}O_3$," *Indian J. Eng. Mater. Sci.*, **15**, 181–6 (2008).

[31]I. D. Raistrick, D. R. Franceschetti, and J. R. Macdonald, "Theory"; pp. 47–8 Chapter 2 in *Impedance Spectroscopy, Theory, Experiment and Application*, 2nd edition, Edited by E. Barsoukov and J. R. Macdonalds. John Wiley & Sons, New York, NY, 2005

[32]J. Liu, C.-G. Duan, W.-G. Yin, W. N. Mei, R. W. Smith, and J. R. Hardy, "Dielectric Permittivity and Electric Modulus in $Bi_2Ti_4O_{11}$," *J. Chem. Phys.*, **119** [5] 2812–9 (2003).

[33]R. Gerhardt, "Impedance and Dielectric Spectroscopy Revisited: Distinguishing Localized Relaxation from Long-Range Conductivity," *J. Phys. Chem. Solids*, **55**, 1491–506 (1994).

[34]O. Bidault, P. Goux, M. Kchikech, M. Belkaoumi, and M. Maglione, "Space-Charge Relaxation in Perovskites," *Phys. Rev. B*, **49** [12] 7868–73 (1994).

[35]C. L. Bull and P. F. McMillan, "Raman Scattering Study and Electrical Properties Characterization of Elpasolite Perovskites Ln₂(BB')O₆ (Ln = La; Sm...Gd and B, B' = Ni, Co, Mn)," *J. Solid State Chem.*, **177**, 2323–8 (2004).

[36]F. S. Galasso, *Structure, Properties and Preparation of Perovskite Type Compounds*. Pergamon Press Ltd, Headington Hill Hall, Oxford, 1969.

[37]B. Scherrer, A. S. Harvey, S. Tanasescu, F. Teodorescu, A. Botea, K. Conder, A. N. Grundy, J. Martynczuk, and L. J. Gauckler, "Correlation Between Electrical Properties and Thermodynamical Stability of $ACoO_{3-\delta}$ Perovskites (A=La, Pr, Nd, Sm, Gd)," *Phys. Rev. B*, **84**, 085113 (2011).

[38]A. K. Jonscher, *Dielectric Relaxation in Solids*. Chelsea-Dielectric Press, London, 1983.

[39]K. S. Rao, D. M. Prasad, P. M. Krishna, B. H. Bindu, and K. Suneetha, "Frequency and Temperature Dependence of Electrical Properties of Barium and Gadolinium Substituted $SrBi_2Ta_2O_9$ Ceramics," *J. Mater. Sci.*, **42** [17] 7363–74 (2007).

[40]S. R. Elliott, "A.C. Conduction in Amorphous Chalcogenide and Pnictide Semiconductors," *Adv. Phys.*, **36** [2] 135–217 (1987).

[41]A. R. Long, "Frequency-Dependent Loss in Amorphous Semiconductors," *Adv. Phys.*, **31** [5] 553–637 (1982).

[42]G. V. Subba Rao, B. M. Wanklyn, and C. N. R. Rao, "Electrical Transport in Rare Earth Orthochromite, Manganites and Ferrites," *Int. J. Phys. Chem. Sol.*, **32**, 345–9 (1971).

[43]D. I. Khomskii and G. A. Sawatzky, "Intermediate-Spin State and Properties of LaCoO₃," *Phys. Rev. B*, **54** [8] 5309–16 (1996).

[44]H. Taguchi, "Spin State of Cobalt in $Nd(Cr_{1-x}Co_x)O_3$," *J. Sol. St. Chem.*, **122**, 297–302 (1996).

[45]R. D. Shannon, "Revised Effective Ionic Radii and Systematic Studies in Halides and Halcogenides," *Acta Crystalogr.*, **32**, 751–6 (1976).

[46]B. A. Boukamp, "A Package for Impedance/Admittance Data Analysis," *Solid State Ionics*, **18–19**, 136–40 (1986).

[47]W. I. Archer and R. D. Armstrong, "The Application of A.C. Impedance Methods to Solid Electrolytes," *Electrochemistry*, Chemical Society Specialist Periodical Reports, **7**, 157–202 (1980).

[48]J. C. Wang and J. B. Bates, "Model for the Interfacial Impedance Between a Solid Electrolyte and a Blocking Metal Electrode," *Solid State Ionics*, **18–19**, 224–8 (1986).

[49]R. D. Armstrong, M. F. Bell, and A. A. Metcalfe, "The AC Impedance of Complex Electrochemical Reactions," *Electrochemistry*, Chemical Society Specialists Periodical Reports, **6**, 98–127 (1978).   □